

# A decentralized frequency and voltage control scheme for grid-forming inverters

Yemi Ojo, Jeremy D. Watson, Khaled Laib and Ioannis Lestas

*Department of Engineering, University of Cambridge, UK*

{yo259, jdw69, kl507, icl20} @cam.ac.uk

**Abstract**—Grid-forming inverters-based autonomous microgrids present new operational challenges as the stabilizing rotational inertia of synchronous machines is absent. We propose in the paper a control architecture for frequency and voltage control with good scalability properties. At slower timescales it allows to incorporate a distributed secondary control policy for which we provide a stability result with line conductances taken into account. At faster timescale this control architecture satisfies a passivity property for a wide range of parameters. The distinctive feature of the voltage control scheme is that it has a double loop structure that uses the DC voltage in the feedback control policy to improve performance. The frequency control policy employs the inverter output current and angle to provide an improved angle droop policy. The performance of the control schemes is illustrated via advanced simulations.

## I. INTRODUCTION

A microgrid can be described as an interconnection of inverter-interfaced distributed generators into a controllable system, which can be operated in grid-connected or autonomous mode. The latter relies on grid-forming inverters for frequency and voltage regulation. Grid-forming inverters do not have the stabilizing rotational inertia as synchronous machines (SMs). Hence these present new operational challenges, and it becomes crucial to design control policies that guarantee the stability of autonomous microgrids.

The design of efficient control schemes for frequency and voltage regulation, and power allocation is still an important problem that is receiving a significant amount of research effort. Existing schemes often have various drawbacks such as steady state frequency deviation, as in e.g. droop control strategies [1]–[3], or inaccurate power allocation at faster timescales as in angle droop control [4]–[7]. Other alternatives based on numerical optimization exist, e.g. the linear matrix inequalities (LMIs) based full-state feedback policies [8], [9], which are single loop schemes, and implemented together with non-droop techniques. [8]. In general, non-droop techniques require that an optimal power flow (OPF) problem is solved for the entire microgrid at predefined intervals and the setpoints transmitted to each inverter [8]. Hence, proportional power sharing cannot be guaranteed during the period between the load change and the new OPF setpoints being communicated. Another approach is passivity based techniques, which allow a decentralized control design with scalability guarantees as in e.g. [9], [3].

This work was supported by the European Research Council (ERC) under Grant 679774.

In this paper we propose a control architecture for frequency and voltage control with good scalability properties. In contrast to single loop strategies e.g. state feedback schemes [8], [9] and more conventional approaches as in [1], [7], our scheme has a double loop structure that uses the DC voltage in the feedback policy to eliminate power imbalance, thereby providing current limiting capabilities and improving DC voltage regulation. Also, we propose a frequency control scheme that exploits the angle dynamics to provide an improved angle droop policy which allows appropriate passivity properties. Furthermore, a distributed secondary control policy at slower timescales is proposed. This achieves power sharing without requiring an OPF to be solved, and is provably stable, under certain design conditions, even when line conductances are taken into account. By contrast, secondary control schemes in the literature usually assume lossless lines to prove stability, e.g. [10], or require an OPF to be solved [8], [9]. Our main contributions are summarized as follows:

- Our control architecture allows to incorporate a distributed secondary control policy at slower timescales for which a stability result can be proven with line conductances taken into account. At faster timescales a passivity property is satisfied for a wide range of parameters.
- The voltage control policy has a double loop structure that uses the DC voltage in the feedback control policy to improve performance. The frequency control scheme uses the inverter output current direct coordinate and angle to provide an improved angle droop.
- We demonstrate the performance of the proposed schemes via advanced simulations.

The remainder of the paper is organised as follows. In section II we give various preliminaries. In section III we describe the frequency and voltage control schemes. A secondary control policy is proposed in section IV. Finally, simulation results are given in section V and conclusions in section VI.

## II. PRELIMINARIES AND MODELS

### A. Notation and Definitions

Let  $\mathbb{R}_{\geq 0} = \{x \in \mathbb{R} | x \geq 0\}$ ,  $\mathbb{R}_{> 0} = \{x \in \mathbb{R} | x > 0\}$ , and  $\mathbb{S} = (-\frac{\pi}{2}, \frac{\pi}{2})$ . Let  $\mathbf{1}_n$  denote the  $n$ -dimensional column vector of ones,  $\mathbf{I}_n$  is the identity matrix of size  $n$ ,  $\mathbf{e} = [1 \ 0]^\top$ ,  $\mathbf{e}_1 = [0 \ 1]^\top$ ,  $\mathbf{e}_2 = \begin{bmatrix} 0 & 1 \\ 0 & 0 \end{bmatrix}$ ,  $J = \begin{bmatrix} 0 & 1 \\ -1 & 0 \end{bmatrix}$  and  $\mathbf{j} = \sqrt{-1}$ . Let  $x = \text{col}(x_1, \dots, x_n) \in \mathbb{R}^n$  denote a column vector with entries  $x_j \in \mathbb{R}$ , and whenever clear from context we use the notation

$x = \text{col}(x_j)$ . We denote  $\text{diag}(a_j)$  an  $n \times n$  diagonal matrix with diagonal entries  $a_j$ , and  $\text{blkdiag}(A_j)$  is a block diagonal matrix with entries  $A_j \in \mathbb{R}^{n \times n}$ . The Kronecker product is denoted by  $\otimes$ , and  $\|A\|_2$  denotes the 2-norm of matrix  $A \in \mathbb{R}^{m \times n}$ . We use the Park transformation, as in [3], to transform a balanced three phase AC signal into its direct-quadrature components. Such quantities at a bus  $j$  in the local reference frame are found by using the local frequency  $\omega_j(t)$  in the transformation, and we refer to these by the lower-case  $dq$  subscript. Similarly, quantities in the common reference frame are found by using a constant common frequency  $\omega_0$  in the transformation, and for such variables we use the upper-case subscript  $DQ$ . The  $dq$  and  $DQ$  frames are related by

$$x_{DQ}(t) = R(\delta(t))x_{dq}(t),$$

$$R(\delta(t)) = \begin{bmatrix} \cos \delta(t) & -\sin \delta(t) \\ \sin \delta(t) & \cos \delta(t) \end{bmatrix}, \quad \delta(t) = \omega(t) - \omega_0, \quad (1)$$

where  $\delta(t) \in \mathbb{S}$  is the angle between the  $dq$  and  $DQ$  reference frames. The time argument  $t$  will often be omitted in the text for convenience in the presentation.

### B. Network model

The network is described by a graph  $(N, E)$  where  $N = \{1, 2, \dots, |N|\}$  is the set of buses, and  $E \subseteq N \times N$  is the set of edges (lines). The grid-forming inverters and loads are connected at the respective buses. The entries of the incidence matrix  $B \in \mathbb{R}^{|N| \times |E|}$  are  $B_{jz} = 1$  if bus  $j$  is the source of edge  $z$  and  $B_{jz} = -1$  if bus  $j$  is the sink of edge  $z$ , with all other elements being zero.  $\mathcal{L} = BB^T \in \mathbb{R}^{|N| \times |N|}$  is the Laplacian matrix. We assume that all the power lines and loads are balanced and symmetric. Consider the  $\pi$ -model of a line connecting a bus  $j \in N$  to a bus  $k \in N$  with resistance and inductance  $R_{jk}, L_{jk} \in \mathbb{R}_{>0}$  and shunt capacitance and conductance  $C_j, G_j \in \mathbb{R}_{>0}$ ; and a resistive-inductive load with parameters  $R_{\ell j}, L_{\ell j} \in \mathbb{R}_{>0}$ . The line and load dynamics in  $DQ$  coordinates are given by

$$C_l \dot{V}_{bDQ} = (-G_l + \omega_0 C_l \mathbf{J}) V_{bDQ} + I_{oDQ} - I_{\ell DQ} - \mathbf{B} I_{lDQ} \quad (2)$$

$$L_l \dot{I}_{lDQ} = (-R_l + \omega_0 L_l \mathbf{J}) I_{lDQ} + \mathbf{B}^T V_{bDQ}$$

$$L_{\ell} \dot{I}_{\ell DQ} = (-R_{\ell} + \omega_0 L_{\ell} \mathbf{J}) I_{\ell DQ} + V_{bDQ} \quad (3)$$

where  $I_{lDQ} = \text{col}(i_{lDQ,jk}) \in \mathbb{R}^{2|E|}$ ;  $V_{bDQ} = \text{col}(v_{bDQ,j})$ ,  $I_{oDQ} = \text{col}(i_{oDQ,j})$ ,  $I_{\ell DQ} = \text{col}(i_{\ell DQ,j}) \in \mathbb{R}^{2|N|}$ ;  $R_l = (\text{diag}(R_{jk}) \otimes \mathbf{I}_2)$ ,  $L_l = (\text{diag}(L_{jk}) \otimes \mathbf{I}_2) \in \mathbb{R}^{2|E| \times 2|E|}$ ;  $C_l = (\text{diag}(C_j) \otimes \mathbf{I}_2)$ ,  $G_l = (\text{diag}(G_j) \otimes \mathbf{I}_2)$ ,  $R_{\ell} = (\text{diag}(R_{\ell j}) \otimes \mathbf{I}_2)$ ,  $L_{\ell} = (\text{diag}(L_{\ell j}) \otimes \mathbf{I}_2)$ ,  $\mathbf{J} = \text{blkdiag}(\mathbf{J}) \in \mathbb{R}^{2|N| \times 2|N|}$ ;  $\mathbf{B} = (B \otimes \mathbf{I}_2) \in \mathbb{R}^{2|N| \times 2|E|}$ ;  $i_{DQ,jk}$ ,  $i_{oDQ,j}$ ,  $i_{\ell DQ,j}$ ,  $v_{bDQ,j}$  are two-dimensional vectors that include the  $DQ$  components of the line current, injected current, load current and bus voltage respectively.

### C. Grid-forming Inverter Model

#### 1) Grid-forming inverter model in local reference frame:

Fig. 1 shows the schematic of a three-phase DC/AC grid-forming inverter. The DC circuit consists of a controllable current source  $i_{dc}$  which takes values in  $\mathbb{R}_{>0}$ , a conductance  $G_{dc} \in \mathbb{R}_{>0}$  and capacitance  $C_{dc} \in \mathbb{R}_{>0}$ . The AC circuit has an  $LCL$  filter with inductances  $L_f, L_c \in \mathbb{R}_{>0}$ , resistances

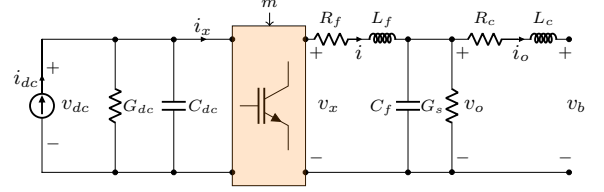


Fig. 1. Grid-forming inverter circuit diagram.

$R_f, R_c \in \mathbb{R}_{>0}$ , a conductance  $G_s \in \mathbb{R}_{>0}$ , and a shunt capacitance  $C_f \in \mathbb{R}_{>0}$ .  $m$  is a balanced three-phase sinusoidal control input signal. We describe the inverter dynamics by its average model since the switching frequency is very high compared to the microgrid frequency and the filter sufficiently attenuates the harmonics. Hence, we consider the inverter model, formulated in the local ( $dq$ ) reference frame, rotating with the local frequency  $\omega_j$ , as in ([3]). To interconnect the inverters with the network (2), it is convenient to transform the  $dq$  model ([3]) to the common ( $DQ$ ) reference frame, rotating at the constant common frequency  $\omega_0$ . Using (1), the representation of the  $dq$  model ([3]) in the  $DQ$  frame is compactly given for the multi-inverter model, with  $m_{DQ} = \mathbf{R}(\delta)m_{dq}$ , as

$$C_{dc} \dot{V}_{dc} = -G_{dc} V_{dc} + I_{dc} - \frac{1}{2} \mathbf{I}_{DQ}^T m_{DQ}, \quad \dot{\delta} = \omega - \omega_0 \mathbf{1}_n$$

$$L_f \dot{I}_{DQ} = (-R_f + \omega_0 L_f \mathbf{J}) I_{DQ} + \frac{1}{2} \mathbf{V}_{dc} m_{DQ} - V_{oDQ} \quad (4)$$

$$C_f \dot{V}_{oDQ} = (-G_s + \omega_0 C_f \mathbf{J}) V_{oDQ} + I_{DQ} - I_{oDQ}$$

$$L_c \dot{I}_{oDQ} = (-R_c + \omega_0 L_c \mathbf{J}) I_{oDQ} + V_{oDQ} - V_{bDQ}$$

where  $\omega = \text{col}(\omega_j)$ ,  $I_{dc} = \text{col}(i_{dc,j})$ ,  $V_{dc} = \text{col}(v_{dc,j}) \in \mathbb{R}^{|N|}$ ;  $\delta = \text{col}(\delta_j) \in \mathbb{S}^{|N|}$ ;  $I_{DQ} = \text{col}(i_{DQ,j})$ ,  $V_{bDQ} = \text{col}(v_{bDQ,j})$ ,  $I_{oDQ} = \text{col}(i_{oDQ,j})$ ,  $m_{dq} = \text{col}(m_{dq,j}) \in \mathbb{R}^{2|N|}$ ;  $C_{dc} = \text{diag}(C_{dc,j})$ ,  $G_{dc} = \text{diag}(G_{dc,j}) \in \mathbb{R}^{|N| \times |N|}$ ;  $R_f = (\text{diag}(R_{fj}) \otimes \mathbf{I}_2)$ ,  $R_c = (\text{diag}(R_{cj}) \otimes \mathbf{I}_2)$ ,  $L_f = (\text{diag}(L_{fj}) \otimes \mathbf{I}_2)$ ,  $L_c = (\text{diag}(L_{cj}) \otimes \mathbf{I}_2)$ ,  $C_f = (\text{diag}(C_{fj}) \otimes \mathbf{I}_2)$ ,  $G_s = (\text{diag}(G_{sj}) \otimes \mathbf{I}_2)$ ,  $\mathbf{V}_{dc} = (\text{diag}(v_{dc,j}) \otimes \mathbf{I}_2)$ ,  $\mathbf{R}(\delta) = \text{blkdiag}(\mathbf{R}(\delta_j)) \in \mathbb{R}^{2|N| \times 2|N|}$ ;  $\mathbf{I}_{DQ} = (\text{diag}(i_{DQ,j}) \otimes \mathbf{e} + \text{diag}(i_{Q,j}) \otimes \mathbf{e}_1) \in \mathbb{R}^{2|N| \times |N|}$ ;  $m_{DQ} = \text{col}(m_{DQ,j}) \in \mathbb{R}^{2|N|}$ ,  $n = |N|$ ;  $i_{DQ,j}$ ,  $i_{oDQ,j}$ ,  $v_{DQ,j}$ ,  $v_{oDQ,j}$  are two-dimensional vectors that include the  $DQ$  components of the inverter currents and voltages respectively.

#### D. Passivity

We review below the notion of passivity, and its use to guarantee microgrid stability in a decentralized way. We use the notion of passivity as defined in [11, Definition 6.3], but with the system state vector  $x$  and input  $u$  replaced by the deviations  $x - x^*$ ,  $u - u^*$  respectively, where  $(x^*, u^*)$  is an equilibrium point. By exploiting the passivity property of the lines when these are represented in  $DQ$  coordinates it can be shown that Assumption 2.1 is a sufficient *decentralized* condition for stability, as stated in Theorem 2.2 (see e.g. [9] where a more advanced line model is also used).

**Assumption 2.1:** Each inverter in the system (4) with state vector  $x = [\delta^T, V_{dc}^T, I_{DQ}^T, V_{oDQ}^T, I_{oDQ}^T]^T$ , input  $u = -V_{bDQ}$  and output  $y = I_{oDQ}$  satisfies the passivity property [11, Definition 6.3] about an equilibrium point  $(x^*, u^*)$ .

**Theorem 2.2 (Closed-loop stability):** Suppose there exists an equilibrium point  $x_m^* = (x_N^*, x^*)$  of the interconnected in-

verter dynamics (4) and network (2), (3), for which the inverter dynamics satisfy Assumption 2.1. Then such an equilibrium point is asymptotically stable.

### III. PROPOSED CONTROL SCHEMES

#### A. Proposed Frequency Control

Grid-forming inverters must operate in a synchronized manner despite load variations and system uncertainties. Our aim is to design a decentralized frequency control scheme that restores frequency to its nominal value after a disturbance, and can be incorporated with a secondary control policy to provide power sharing capabilities.

To this end, we propose a frequency control scheme that can be seen as an improved angle droop policy that leads to passivity properties in the  $DQ$  frame. This scheme takes the inverter output current  $I_{oD} := \mathbf{e}^\top I_{oDQ}$  (i.e., the first component of  $I_{oDQ}$ ) and the angle  $\delta$  as feedback to adapt the frequency as described below:

$$\omega = \omega_0 \mathbf{1}_n - k_p \mathbf{e}^\top I_{oDQ} - k_I \delta + \chi \quad (5)$$

where  $k_p = \text{diag}(k_{p,j})$ ,  $k_I = \text{diag}(k_{I,j}) \in \mathbb{R}_{>0}^{[N] \times [N]}$  are the matrices of the droop and damping gains respectively,  $\mathbf{e} = (\mathbf{I}_n \otimes \mathbf{e}) \in \mathbb{R}^{2[N] \times [N]}$ , and  $\chi = \text{col}(\chi_j) \in \mathbb{R}^{[N]}$  are set-points. Considering (5) with the  $\dot{\delta}$  in (4) results in an improved version of angle droop where the term  $k_I \delta$  provides the necessary damping of the angle dynamics which helps the inverter model (5) to satisfy a passivity property in the  $DQ$  frame (discussed in section V-A). The current  $I_{oD}$  allows to achieve power sharing by appropriately adjusting  $\chi$ , and the choice of  $k_p$  sets the power sharing ratio (section IV). The parameters  $\chi$  are assumed to be transmitted to each inverter by secondary control.  $\chi$  can provide additional capability to correct clock drifts which may arise due to clock inaccuracies as discussed in [4]. Furthermore, considering (5) with the  $\dot{\delta}$  in (4) the frequency of each inverter at equilibrium equals the common constant frequency, i.e.  $\omega^* = \omega_0 \mathbf{1}_n$  (section V).

A further benefit of our proposed controller (5) is that it provides inertia and damping similar to the dynamic behaviour of the SM, which is not achievable with traditional angle droop control [4]–[7]. To show this, substitute (5) into the  $\dot{\delta}$  dynamics in (4), to give

$$M \dot{\delta} = -D \delta - \mathbf{e}^\top I_{oDQ} + M \chi_j, \quad (6)$$

where  $M = k_p^{-1}$ ,  $D = k_p^{-1} k_I$ . Equation (6) is analogous to a swing equation, with the frequency replaced by the angle  $\delta$ .  $M$  corresponds to the inertia, and  $D$  the damping coefficient. The droop gains  $k_p$  can be chosen to shape the desired (virtual) inertia  $M$ , and  $k_I$  provides an additional degree of freedom to design  $D$ . This is an improvement compared to the traditional angle droop control [4]–[7] where the inertia  $M$  is zero and only  $k_p$  is available to design  $D$ .

#### B. DC voltage regulation

To ensure DC voltage regulation we present a DC voltage proportional-integral (PI) controller

$$I_{dc} = -\Lambda_P (V_{dc} - \mathbf{1}_n v_{dc,r}) - \Lambda_I \zeta, \quad \dot{\zeta} = V_{dc} - \mathbf{1}_n v_{dc,r}, \quad (7)$$

where  $\zeta = \text{col}(\zeta_j) \in \mathbb{R}^{[N]}$  is the integrator state,  $\Lambda_P = \text{diag}(\Lambda_{P,j})$ ,  $\Lambda_I = \text{diag}(\Lambda_{I,j}) \in \mathbb{R}_{>0}^{[N] \times [N]}$  are the proportional and integral gains respectively.

#### C. Inverter output voltage regulation

Grid-forming inverters must regulate the voltage of the grid they form, hence they need to have voltage regulation capability. This is achieved in our proposed scheme via the control signal  $m_{DQ}$  in (4). In particular, we follow the standard double loop design where the inner loop is faster than the outer one. One distinctive feature of our scheme is that it uses the DC voltage to eliminate power imbalance in the inner loop. First, the reference current  $i_{DQ,j}^r$  is generated by the outer voltage loop by means of PI control acting on the voltage deviation  $v_{oDQ,j} - R(\delta_j) \mathbf{e} V_n - n_{q,j} \mathbf{e}_2 i_{oDQ,j}$ . We use  $-n_{q,j} \mathbf{e}_2 i_{oDQ,j} = -n_{q,j} i_{oQ,j}$  to adjust the direct-coordinate of  $R(\delta_j) \mathbf{e} V_n$ , similar to the conventional reactive power based voltage droop control in [1], [7]. Then, the inner control loop generates  $m_{DQ,j}$  by means of PI control acting on the power imbalance  $i_{DQ,j} v_{dc,r} - i_{DQ,j}^r v_{dc,j}$ . The compact form of the voltage control scheme is given by

$$\begin{aligned} \dot{\beta}_{DQ} &= V_{oDQ} - \mathbf{R}(\delta) \mathbf{e} V_n - \underline{n}_q I_{oDQ} \\ I_{DQ}^r &= -c_p (V_{oDQ} - \mathbf{R}(\delta) \mathbf{e} V_n - \underline{n}_q I_{oDQ}) - c_I \beta_{DQ} \\ \dot{\xi}_{DQ} &= \mathbf{I}_{DQ} \mathbf{1}_n v_{dc,r} - \mathbf{I}_{DQ}^r V_{dc} \\ m_{DQ} &= -\lambda_P (\mathbf{I}_{DQ} \mathbf{1}_n v_{dc,r} - \mathbf{I}_{DQ}^r V_{dc}) - \lambda_I \xi_{DQ}. \end{aligned} \quad (8)$$

where  $\beta_{DQ} = \text{col}(\beta_{DQ,j})$ ,  $\xi_{DQ} = \text{col}(\xi_{DQ,j})$ ,  $I_{DQ}^r = \text{col}(i_{DQ,j}^r) \in \mathbb{R}^{2[N]}$ ;  $c_p = (\text{diag}(c_{p,j}) \otimes \mathbf{I}_2)$ ,  $\lambda_P = (\text{diag}(\lambda_{P,j}) \otimes \mathbf{I}_2)$ ,  $c_I = (\text{diag}(c_{I,j}) \otimes \mathbf{I}_2)$ ,  $\lambda_I = (\text{diag}(\lambda_{I,j}) \otimes \mathbf{I}_2)$ ,  $\underline{n}_q = \text{blkdiag}(\mathbf{e}_2 n_{q,j}) \in \mathbb{R}_{>0}^{2[N] \times 2[N]}$ ;  $\mathbf{I}_{DQ}^r = (\text{diag}(i_{D,j}^r) \otimes \mathbf{e} + \text{diag}(i_{Q,j}^r) \otimes \mathbf{e}_1) \in \mathbb{R}^{2[N] \times [N]}$ ;  $V_n \in \mathbb{R}_{>0}$  is the nominal voltage,  $n_{q,j} \in \mathbb{R}_{>0}$  is the voltage droop gain.

### IV. SECONDARY CONTROL SCHEME

Here we discuss the active power sharing that (5) can provide when  $\chi$  is updated via the distributed scheme described below, which can be seen as a secondary control policy occurring at slower timescales:

$$\dot{\chi} = -\alpha \mathcal{L} \chi + \alpha \mathcal{L} k_I \delta. \quad (9)$$

where  $\alpha > 0$ . The power sharing property achieved by (9) at equilibrium is stated below (proof given in the Appendix).

**Proposition 4.1 (Power sharing):** At equilibrium the dynamics given by (2)–(5), (7)–(9) satisfy

$$\frac{I_{oD,j}^*}{I_{oD,k}^*} = \frac{k_{p,k}}{k_{p,j}}, \quad \forall j, k \in N. \quad (10)$$

**Remark 4.2:** (10) gives approximate power sharing at equilibrium. Given the active power  $P_{o,j}^* := V_{oD,j}^* I_{oD,j}^*$ ,  $\forall j \in N$  and (10), the power sharing ratio between inverter  $j, k \in N$  is

$$\frac{P_{o,j}^*}{P_{o,k}^*} = \frac{V_{oD,j}^* I_{oD,j}^*}{V_{oD,k}^* I_{oD,k}^*} = \frac{V_{oD,j}^*}{V_{oD,k}^*} \frac{k_{p,k}}{k_{p,j}}, \quad \forall j, k \in N. \quad (11)$$

If  $V_{oD,j}^* = V_{oD,k}^*$ , which is a property that approximately holds since the voltage does not vary much compared to its nominal value, the active power is proportionally shared

among the inverters according to the ratio  $k_{pk}/k_{pj}$ .  $k_{p,j}$  are chosen inversely proportionally to the inverter ratings.

It can be shown that the equilibrium point is also locally asymptotically stable under an assumption of timescale separation between the secondary control and the inverter/network dynamics. For the analysis below we assume that  $\chi$  is updated at a much slower timescale (e.g. 100 ms) than the inverter and line dynamics (typically about 1 ms) such that in this timescale (2)–(5), (7), (8) is assumed to have reached equilibrium, thus we obtain the linearized static model (12).

$$\tilde{\delta} = -(k_I k_p^{-1} + F(\delta^*) V_n)^{-1} k_p^{-1} \tilde{\chi} \quad (12)$$

where  $F(\delta^*) = \mathbf{e}^\top Y_2 \mathbf{J}^\top \mathbf{R}(\delta^*) \mathbf{e}$ ,  $Y_2 = ((R_c - \omega_0 L_c \mathbf{J}) + Y_1^{-1} - \underline{n}_q)^{-1}$ ,  $Y_1 = (G_l - \omega_0 C_l \mathbf{J}) + (R_\ell - \omega_0 L_\ell \mathbf{J})^{-1} + \mathbf{B}(R_l - \omega_0 L_l \mathbf{J})^{-1} \mathbf{B}^\top$ . Linearizing (9) around  $(\chi^*, \delta^*)$  gives

$$\dot{\tilde{\chi}} = -\alpha \mathcal{L} \tilde{\chi} + \alpha \mathcal{L} k_I \tilde{\delta}. \quad (13)$$

We now state the stability result. Its proof is in the Appendix. In the theorem we make use of the following quantity:

$$\mathcal{M}(\delta^*) = \mathbf{I}_n + k_I (k_I k_p^{-1} + F(\delta^*) V_n)^{-1} k_p^{-1}. \quad (14)$$

**Theorem 4.3:** Consider the system (12), (13) and  $\mathcal{M}(\delta^*)$  as in (14). Suppose  $|\delta_j^*| < \pi/2$ ,  $\forall i \in N$ , and  $k_{p,j}$ ,  $k_{I,j}$ ,  $\forall j \in N$  are selected such that  $\tau = k_{I,j}/k_{p,j} \forall j \in N$ , for some  $\tau > 0$ . When  $|\delta_j^*|$  are sufficiently small at an equilibrium point of the interconnected system, then this is locally asymptotically stable. In particular, asymptotic stability is guaranteed if

$$\|\Delta\|_2 < K^{-1} \lambda_{n-1}(H) \quad (15)$$

where  $\Delta = \mathcal{L}(\mathcal{M}(\delta^*) - \mathcal{M}(\mathbf{0}_n))$ ,  $H = \mathcal{L}\mathcal{M}(\mathbf{0}_n)$  and  $K = \|V^{-1}\|_2 \|V\|_2$  is the condition number of  $H$ , where  $V$  is its diagonalizing eigenbasis, and  $\lambda_{n-1}(H)$  is its second smallest eigenvalue (all eigenvalues of  $H$  are real).

**Remark 4.4:** The upper bound in (15) can easily be computed as  $\mathcal{L}$  and  $\mathcal{M}(\mathbf{0}_n)$  are known matrices. It should also be noted that in the example given in section V, this condition is only slightly conservative and is easily satisfied (with considerable margin) for all realistic values of  $\delta^*$ .

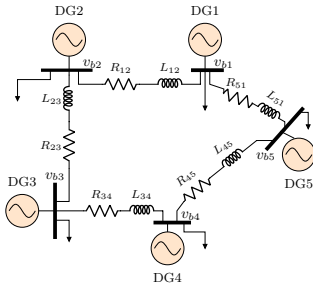


Fig. 2. An autonomous inverter-based microgrid consisting of five grid-forming inverters. The sign  $\downarrow$  denotes loads.

## V. SIMULATION RESULTS

In this section we assess numerically the passivity of the inverters and illustrate via simulations their performance.

### A. Passivity assessment of inverters

We investigate whether the passivity property stated in Assumption 2.1, i.e. a decentralized condition for stability, is sat-

TABLE I  
MICROGRID PARAMETERS

Description	Value
Inverter parameters	$R_{fj}=0.1 \Omega$ , $L_{fj}=5 \text{ mH}$ , $C_{fj}=50 \mu\text{F}$ , $C_{dc,j}=10 \text{ mS}$ , $R_{cj}=0.2 \Omega$ , $L_{cj}=2 \text{ mH}$ , $G_{dc,j}=10 \text{ mS}$ , $G_{sj}=3 \text{ mS}$
Controller parameters	$\omega_0 = 2\pi(50) \text{ rad/s}$ , $v_{dc,r}=10^3 \text{ V}$ , $V_n=311 \text{ V}$ , $\alpha = 667$ , $k_{p,j}=0.06$ , $n_{q,j}=0.078$ , $k_{I,j}=40$ , $c_{p,j}$ , $\Lambda_{P,j}=1$ , $c_{I,j}$ , $\Lambda_{I,j}=10$ , $\lambda_{P,j} = 1/v_{dc,r}$ , $\lambda_{I,j} = 25/v_{dc,r}$
Loads parameters	$R_{\ell,1}, R_{\ell,2}, R_{\ell,3}=20 \Omega$ , $R_{\ell,4}, R_{\ell,5}=25 \Omega$ , $L_{\ell,1}, L_{\ell,3}=30 \text{ mH}$ , $L_{\ell,2}, L_{\ell,4}=40 \text{ mH}$ , $L_{\ell,5}=20 \text{ mH}$ , 3.0 kW/0.5 kVar at bus 1
Switched loads	2.5 kW at buses 1, 2, 3 & 4
Line parameters	$R_{12}=0.2 \Omega$ , $R_{45} = 0.15 \Omega$ , $R_{23}, R_{34}, R_{51}=0.1 \Omega$ , $L_{12}, L_{34} = 4 \text{ mH}$ , $L_{23}=2.8 \text{ mH}$ , $L_{45}=3.5 \text{ mH}$ , $L_{51}=3 \text{ mH}$ , $C_j=0.1 \mu\text{F}$ , $G_j=1 \text{ mS}$
Conventional scheme	$k_{p,j}=0.06/311$ , $n_{q,j}=0.078/311$ , $K_{pv}=5$ , $K_{iv}=10$ , $K_{pi}=2$ , $K_{ii}=15$

TABLE II  
EQUILIBRIUM VALUES

$\delta_1^*=-0.0231$ , $\delta_2^*=-0.0162$ ; $I_{DQ1}^*=(14.3,-3.18)$ , $I_{DQ2}^*=(14.2,-2.73)$ ; $V_{oDQ1}^*=(310,-3.55)$ , $V_{oDQ2}^*=(311,-5.04)$ ; $I_{DQ1}^*=(13.4,-7.83)$ , $I_{DQ2}^*=(13.2,-7.39)$ ; $m_{DQ1}^*=(0.33,0.036)$ , $m_{DQ2}^*=(0.33,-0.037)$ .
$\delta_1^*=-0.0194$ , $\delta_2^*=-0.0192$ , $\delta_3^*=-0.0254$ , $\delta_4^*=-0.025$ , $\delta_5^*=-0.0268$ ; $I_{DQ1}^*=(14.7,-1.06)$ , $I_{DQ2}^*=(14.6,-0.633)$ , $I_{DQ3}^*=(14.6,-1.14)$ , $I_{DQ4}^*=(14.6,-0.367)$ , $I_{DQ5}^*=(14.6,-0.129)$ ; $V_{oDQ1}^*=(310,-8.55)$ , $V_{oDQ2}^*=(311,-6.14)$ , $V_{oDQ3}^*=(310,-8.08)$ , $V_{oDQ4}^*=(311,-4.32)$ , $V_{oDQ5}^*=(311,-5.41)$ ; $I_{DQ1}^*=(13.7,-5.97)$ , $I_{DQ2}^*=(13.7,-5.57)$ , $I_{DQ3}^*=(14.6,-1.14)$ , $I_{DQ4}^*=(13.7,-5.11)$ , $I_{DQ5}^*=(13.7,-4.41)$ ; $m_{DQ1}^*=(0.35,0.078)$ , $m_{DQ2}^*=(0.35,-0.077)$ , $m_{DQ3}^*=(0.36,0.057)$ , $m_{DQ4}^*=(0.36,0.070)$ , $m_{DQ5}^*=(0.35,0.079)$

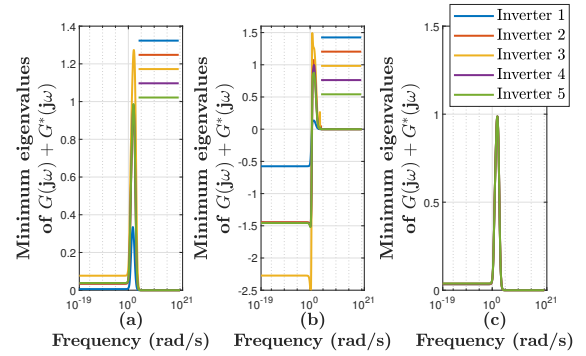


Fig. 3. Passivity of grid-forming inverters: (a) with proposed control scheme; (b) with conventional frequency droop and voltage scheme [1]; (c) with proposed control scheme for the example presented in section V-B

isfied with the proposed control scheme (5), (7), (8). We consider a fast timescale, i.e. the secondary control parameter  $\chi$  is taken as constant, since this is adjusted at slower timescales. Passivity is numerically assessed via the KYP Lemma [11] which requires  $G(j\omega) + G^*(j\omega) \geq 0$  for all frequencies, where  $G(j\omega)$  is the frequency response matrix of the linearization of (4), (5), (7), (8) with input  $\tilde{u} = -\tilde{V}_{bDQ}$  and  $\tilde{y} = \tilde{I}_{oDQ}$ . The test is performed on various benchmark examples in [3], [4], [6], [7], [12] commonly used in the literature to validate control policies for grid-forming inverters. Table II presents a set of realistic equilibrium points typical for inverters with rating 10-15 kVA around which the analysis can be performed. Fig. 3(a) shows the passivity assessment with the proposed scheme, where each plot corresponds to benchmark examples in [3], [4], [6], [7], [12], and this is compared to that with the conventional frequency and voltage scheme [1] shown in Fig. 3(b). Fig. 3(a) shows that the minimum eigenvalue of  $G(j\omega) + G^*(j\omega)$  is non-negative over all frequencies, thus validating that the inverters in these examples satisfy the passivity property for appropriate values of  $k_{I,j}$ , in contrast

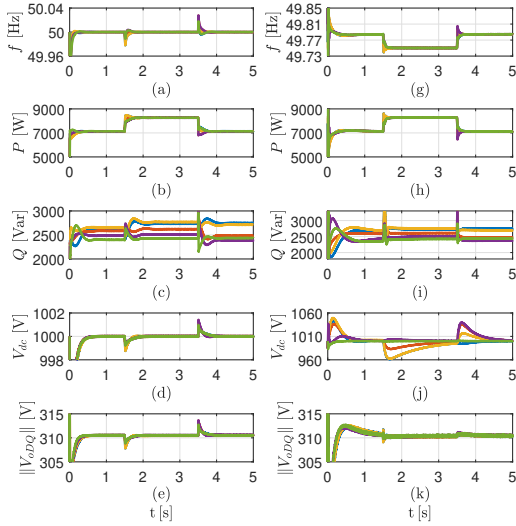


Fig. 4. System response with proposed control:(a)–(e); System response with conventional frequency droop and voltage scheme in [1]:(g)–(k); Inverter 1 ‘-’, Inverter 2 ‘-’, Inverter 3 ‘-’, Inverter 4 ‘-’, Inverter 5 ‘-’.

to those with conventional schemes shown in Fig. 3(b). We also tested the proposed scheme on a five-inverter system presented in section V-B, with validation of the passivity property illustrated in Fig. 3(c).

### B. Numerical simulation

We show via simulations in MATLAB / Simscape Electrical the performance of the proposed control policy (5), (7)–(9). Fig. 2 shows the five-inverter test system, and Table I presents the system parameters where the subscript  $j=1, \dots, 5$ . The simulation model is detailed and realistic, and includes the PWM switching of the inverters. The values of  $k_{I,j}, k_{p,j}$  satisfy the selections in Proposition 4.3. The performance of the proposed scheme is compared to that with conventional frequency droop and voltage control, as in [1], in the presence of disturbances: a 2.5 kW load is switched on at buses 1 and 3 at  $t = 1.5$  s, and an equivalent load is switched off at buses 2 and 4 at  $t = 3.5$  s. All other loads are connected to the corresponding buses throughout the simulation. The response with the proposed control scheme is shown in Fig. 4(a)–(e), and that with the conventional frequency droop and voltage scheme [1] shown in Fig. 4(g)–(k). The frequencies synchronize to  $\omega_0/2\pi$  Hz, in contrast to the conventional frequency droop that has steady-state frequency deviation. The active power sharing with communication agrees with Proposition 4.1. The proposed control scheme also distributes the reactive power and shows improvement in the transient response. Since the proposed voltage scheme uses the DC voltage in its feedback control policy, its response shows significant improvement in the DC voltage regulation, in contrast to the conventional voltage scheme [1]. The output voltages satisfy the typical requirement  $0.9V_n < \|V_{oDQ,j}\| < 1.1V_n, \forall j \in N$ .

## VI. CONCLUSION

We have proposed a control architecture for frequency and voltage control with good scalability properties. At slower

timescales it allowed to incorporate a secondary control policy which is provably stable with line conductances considered. At faster timescale it offered passivity properties for a wide range of parameters. The voltage control scheme has a double loop structure that uses the DC voltage in the feedback control policy to improve performance. The frequency control policy uses the inverter output current and angle to provide an improved angle droop. Simulations on advanced models showed that the control schemes lead to good transient performance.

## REFERENCES

- [1] N. Pogaku, M. Prodanovic, and T. C. Green, “Modeling, analysis and testing of autonomous operation of an inverter-based microgrid,” *IEEE TPE*, 22, 2, 2007.
- [2] C. Arghir, T. Jouini, and F. Dörfler, “Grid-forming control for power converters based on matching of synchronous machines,” *Automatica*, vol. 95, 2018.
- [3] Y. Ojo, M. Benmiloud, and I. Lestas, “Frequency and voltage control schemes for three-phase grid-forming inverters,” *IFAC-PapersOnLine*, 2020.
- [4] R. R. Kolluri, I. Mareels, T. Alpcan, M. Brazil, J. de Hoog, and D. A. Thomas, “Power sharing in angle droop controlled microgrids,” *IEEE TPS*, 32, 6, 2017.
- [5] R. Majumder, A. Ghosh, G. Ledwich, and F. Zare, “Angle droop versus frequency droop in a voltage source converter based autonomous microgrid,” in *2009 IEEE PES GM*, 2009.
- [6] R. Majumder, G. Ledwich, A. Ghosh, S. Chakrabarti, and F. Zare, “Droop control of converter-interfaced microsources in rural distributed generation,” *IEEE TPD*, 25, 4, 2010.
- [7] Y. Sun, X. Hou, J. Yang, H. Han, M. Su, and J. M. Guerrero, “New perspectives on droop control in ac microgrid, 64, 7,” *IEEE TIE*, 2017.
- [8] M. S. Sadabadi, Q. Shafiee, and A. Karimi, “Plug-and-play voltage stabilization in inverter-interfaced microgrids via a robust control strategy,” *IEEE TCST*, 25, 3, 2016.
- [9] J. Watson, Y. Ojo, K. Laib, and I. Lestas, “A scalable control design for grid-forming inverters in microgrids,” *accepted, IEEE TSG*, 2021.
- [10] J. W. Simpson-Porco, F. Dörfler, and F. Bullo, “Synchronization and power sharing for droop-controlled inverters in islanded microgrids,” *Automatica*, 49, 9, 2013.
- [11] H. K. Khalil, *Nonlinear control*. Pearson New York, 2015.
- [12] J. M. Guerrero, L. G. De Vicuna, J. Matas, M. Castilla, and J. Miret, “A wireless controller to enhance dynamic performance of parallel inverters in distributed generation systems,” *IEEE TPE*, 19, 1, 2004.
- [13] F. L. Bauer and C. T. Fike, “Norms and exclusion theorems,” *Numerische Mathematik*, 2, 1, 1960.
- [14] M. Zedek, “Continuity and location of zeros of linear combinations of polynomials,” *Proceedings of the AMS*, 16, 1, 1965.

## APPENDIX

*Proof of Proposition 4.1* At equilibrium we have  $\mathbf{0}_n = \mathcal{L}k_p \mathbf{e}^\top I_{oDQ}^*$ , which holds if and only if  $k_p \mathbf{e}^\top I_{oDQ}^* = k_p I_{oD}^* = \bar{\kappa} \mathbf{1}_n$ , for some  $\bar{\kappa} > 0$ . The latter implies (10).

*Proof of Theorem 4.3:* Substituting (12) in (13) gives

$$\dot{\tilde{\chi}} = -\alpha \mathcal{LM}(\delta^*) \tilde{\chi} \quad (16)$$

With  $\tau$  as in Theorem 4.3,  $\mathcal{M}(\mathbf{0}_n)$  is positive definite.  $H$  (i.e.  $\mathcal{LM}(\mathbf{0}_n)$ ) is diagonalizable [13] and has a single zero eigenvalue and the rest strictly positive.  $\mathcal{LM}(\delta^*)$  always has the same single zero eigenvalue, and since the eigenvalues vary continuously with  $\delta^*$  [14], there exist sufficiently small values of  $\delta^*$  such that the eigenvalues of  $\mathcal{LM}(\delta^*)$  are non-negative. Suppose the second smallest eigenvalue of  $H$ ,  $\lambda_{n-1}(H)$ , satisfies condition (15). Then, from an application of the Bauer-Fike theorem on  $\Delta + H$  it can be deduced that all other eigenvalues of  $\mathcal{LM}(\delta^*)$  are strictly positive and hence (16) is asymptotically stable.